Pathogenicity of Commensal Gut Biofilm In Prefrail Aging

Guillaume Le Cosquer[1,2], Melissa Pannier[1], Elodie Meunier[1], Julie Thevenin[1], Elise Pyhourquet[1], Sophie Guyonnet[3,*], Bruno Vellas[3,*], Yohan Santin[4,*], Bruno Guiard[5,*], Angelo Parini[4,*], Louis Buscail[2], Barbara Bournet[2], Damien Guillemet[6], Celine Deraison[1], Nathalie Vergnolle[1,7,#,*], Jean-Paul Motta[1,#,*,✉] *for the IHU HealthAge INSPIRE/Open Science study group*

Affiliations:

[1]Institute of Digestive Health Research (IRSD), INSERM, Toulouse University, INRAe, ENVT, University Toulouse III Paul Sabatier (UPS), 31300 Toulouse, France

[2]Department of Gastroenterology and Pancreatology, Toulouse University Hospital (CHU Toulouse), Toulouse, France and Toulouse University, University Toulouse III Paul Sabatier (UPS), 31059 Toulouse, France

[3] Institute of Aging, Toulouse University Hospital (CHU Toulouse), Toulouse, France and CERPOP, Toulouse University, INSERM, University Toulouse III Paul Sabatier (UPS), 31300 Toulouse, France

[4] Institute of Metabolic and Cardiovascular Diseases (I2MC), INSERM, Toulouse University, University Toulouse III Paul Sabatier (UPS), 31432, Toulouse, France

[5] Research Center on Animal Cognition (CRCA), Center of Integrative Biology (CBI), Université de Toulouse, CNRS UMR-5169, Univ Toulouse III - Paul Sabatier (UPS), Toulouse, France.

[6] Nexira, 129 Chemin de Croisset, 76000 Rouen, France

[7] Department of Physiology and Pharmacology, University of Calgary Cumming School of Medicine, 3330 Hospital Drive, NW Calgary, AB, T2N4N1, Canada

* members of the IHU HealthAge INSPIRE/Open Science study group (full list in supplementary material)

[#] Co-supervision

✉Correspondence to: jean-paul.motta@inserm.fr

Keywords: gut microbiota; aging; microb-aging; gut biofilm; prefrailty; geroscience

Main text – ≈ 6.700 words or ≈38.000 characters, excluding Title Page, Tables, Figures, and References

Abstract – 149 words

Display items – 6 Figures + 1 Table

Running title: Pathogenicity of prefrail gut biofilms

Abstract. Pathophysiological mechanisms of unhealthy aging, particularly the transition from robustness to frailty, remain poorly understood. Despite extensive microbiome research on taxonomy, the behavior of early prefrail gut bacteria in their natural community-host mucosal tissue context remains unexplored. Using fecal samples from the INSPIRE-T aging human cohort, we characterized gut microbiota phenotype during prefrailty stages using a polymicrobial biofilm model. Results revealed that prefrail-derived biofilms exhibited distinct taxonomic and physical alterations, enhanced dispersal, and increased epithelial virulence compared to robust counterparts. Multiparametric analyses linked biofilm characteristics to clinical traits, suggesting their potential as aging status indicators. Polyphenol-rich grape pomace extract partially reversed prefrail biofilm alterations and reduced proinflammatory prefrail biofilm responses *in vitro*. Microbiota from prefrail aged mice induced colon damage in antibiotic-treated recipients, establishing a prefrail microbiome-inflammation causality. Overall, the findings identified novel prefrail microbiome characteristics, established causal inflammatory links, and support microbiota-targeted geroprotective interventions for the prefrail populations.

1. INTRODUCTION

By 2030, the World Health Organization (WHO) projects that one in six individuals worldwide will be aged 60 years or older [1]. This shift to older populations coincides with an increase in age-associated diseases and unhealthy aging. One of the first steps in the development of unhealthy aging is linked to the appearance of frailty syndrome, a clinical condition defined as decreased physiological reserve and function that heightens vulnerability and impairs the ability to withstand health stresses[2]. The absence of frailty (robust individuals) has been identified as a reliable predictor of prolonged longevity without age-associated diseases [3]. The field of geroscience, which has recently emerged, is dedicated to understanding the underlying mechanisms of aging, finding methods to extend the healthspan – rather than lifespan – and to delay or impede frailty syndrome and age-associated diseases [4]. The scientific community has intensely focused on describing fecal microbiome composition and changes in the aging population[5-8]. From these studies, it has become clear that chronological age is linked to alterations within the gut microbiome, a process coined as 'microb-aging' by Bosco and Noti[6]. A current challenge is to identify additional aspects of microb-aging, beyond taxonomy, that could be related to early signs of unhealthy aging (in prefrail individuals)[9]. The involvement of microbiota behavior and virulence in such differences has not yet been investigated. Although clinical scales allow geroclinicians to categorize patients into three categories according to their frailty status (robust, prefrail, and frail individuals), biological data on the relationship between these progressive clinical changes and microb-aging dynamics are scarce. From a clinical perspective, prefrail individuals represent a potentially reversible stage before a significant decline in health. A report on community-dwelling elders indicated a notable prefrailty-to-robust transition, with a 16% conversion rate observed over an 18-to 36-month follow-up

73 period, compared to 0% during the same period for the frailty-to-robust transition [10]. Defining
74 conditions or treatments that would favor this transition from prefrailty-to-robust is among
75 the most important challenge of geroscience[10].

76 The motivation of this study was thus to focus on the aging population exhibiting prefrail
77 characteristics, in the search for interventions seeking at prefrailty-to-robust transition. For
78 that, we capitalized on the French INSPIRE-T cohorts at Toulouse University Hospital, two
79 clinically well-characterized human and mouse aging cohorts in which various non-invasive
80 samples were collected, including fecal samples. These cohorts were designed to identify
81 novel markers of aging, age-related diseases and health evolution that could be
82 therapeutically targetable[11-13]. Considering its key importance on gut health and disease, we
83 aimed at focusing on microbiota communities living on the surface of the mucosa, as a
84 polymicrobial anaerobic biofilm[14]. To that end, we used a static model of polymicrobial
85 biofilms grown on mucin-coated polystyrene microplates (MBEC device model[15-17]), providing
86 a straightforward, mid-throughput system for parallel community analysis. Our underlying
87 hypothesis was that these cultured biofilms, while partially preserving the fecal taxonomy,
88 and could retain key structural and phenotypic alterations associated with both aging and
89 donor health status. Ultimately, our goal was to establish a proof-of-concept platform for
90 geroprotective experimental strategies aimed at addressing these abnormalities.

91 **2. METHODS**

92 *Human clinical data and samples*

93 This study used human feces collected from the INSPIRE-T cohort in 2021 (ID
94 NCT04224038, Table 1 and Supplementary Table 1)[12]. Donors were categorized into groups
95 of 13 adults (7 men/6 women; 30-70 years) and 29 elderly subjects (+ 70 years). The last group

96 was divided into 14 prefrail (6 men/8 women) and 15 healthy or robust individuals (7 men/8
97 women). Frailty syndrome was evaluated using the Fried frailty index (Supplementary Table
98 2 for detailed Fried index calculation[2]). Donors were excluded if they had received antibiotics,
99 probiotics, or prebiotics within the past three months and if they had history of any of the
100 following conditions: inflammatory bowel disease, irritable bowel syndrome, colorectal
101 cancer, immunosuppression, severe liver disease. Feces were collected at the initial visit,
102 aliquoted (≈1 g), and stored at −80°C until analysis in the INSPIRE-T biobank at a central
103 laboratory (Toulouse Bio Ressources CRB, CHU Toulouse/IFB Purpan, Toulouse, France).
104 Clinical characteristics, including age, gender, frailty status, and household status, were
105 documented (Supplementary Table 1: lifestyle). For the present analysis, we used the version
106 1.0 of the INSPIRE-T database. We calculated the nutritional status of each individual using
107 the Mini Nutritional Assessment (MNA; Supplementary Tables 3 and 4[18]) and calculated the
108 Charlson Comorbidity Index based on their past medical history[19](Supplementary Tables 5,
109 S6, and S7). Full list of members of the IHU HealthAge INSPIRE/Open Science study group is
110 included in Supplementary Material.

111 *Mouse functional data and samples*

112 This study involved colon tissue and feces collected from the INSPIRE mice cohort (CREFRE
113 – US006 / Inserm – University of Toulouse, Paul Sabatier). The cohort comprised male and
114 female SWISS outbred mice[13]. Animals underwent health assessments to measure frailty,
115 using a rodent equivalent to the human Fried frailty index, the Valencia Score[13,20]
116 (Supplementary Table 8). Behavioral phenotyping was conducted by the Mouse Behavioral
117 Core platform (Integrative Biology Center, CBI, Toulouse), at the CREFRE facility. In this study,
118 we collected samples from young (6 months, n=8), aged robust (24 months, n=8), and aged
119 prefrail animals (24 months, n=8). Distal colon was fixed in methacarn solution (6/3/1 of

120 methanol/chloroform/acetic acid), and embedded in paraffin. Feces were collected and
121 stored at −80°C. Both paraffin blocks and frozen feces were maintained in the INSPIRE mouse
122 biobank at a central laboratory (Centre de Ressources Biologiques-Cancer - Institut
123 Universitaire du Cancer Toulouse – Oncopole, CHU Toulouse, Toulouse, France).

124 *Culture of biofilms from human feces*

125 Human fecal samples (10-20 mg) were resuspended in supplemented Brain Heart Infusion
126 (BHI; Sigma-Aldrich 53286, St. Quentin Fallavier, France), enriched with hemin solution (final
127 5 µg/ml; Sigma-Aldrich H9039), Vitamin K1 (final 50µg/ml; Sigma-Aldrich V3501), and L-
128 Cysteine (0.5 mg/ml; Sigma-Aldrich W326305). Human microbiota biofilms was grown in
129 mucin-coated polystyrene pegs of MBEC Biofilm plates (Innovotech, Edmonton, AB, Canada)
130 by incubating the lids in a solution of 10mg/ml gastric porcine mucin (Sigma-Aldrich M1778,
131 a crude porcine mucin type III preparation, bound with sialic acid 0.5-1.5%) overnight at room
132 temperature without agitation (based on methods first described in [21]). After mucin-coating,
133 the lids were place onto another 96-well plate containing BHI supplemented and dilution of
134 fecal microbiota (OD 600nm =0.1; Varioskan® Flash, Thermo Scientific Massachusetts, MA,
135 USA). Biofilms were then matured for 72 hours in a humidified incubator set at 37 °C, under
136 anaerobic condition and continuous rocking (Rocker25 from Labnet set at 50 RPM) as
137 described in[15-17]. After maturation, the lid was gently rinsed and basal BHI plate was refreshed
138 to collect naturally dispersed bacteria from biofilms under the same conditions for an
139 additional 24 hours. Biofilm biomass, viability, and matrix content were characterized using
140 the methods described below. Additionally, the basal plate medium containing biofilm-
141 dispersed bacteria were collected and was used for 16S rRNA V3-V4 gene sequencing, to
142 estimate dispersal rates, and to perform interaction assays with human intestinal epithelial
143 cells. For all microbiological procedures described herein, original sample handling and

144 incubations were carried out in an anaerobic chamber (Don Whitley A20, 0.1% oxygen; 4.9%
145 CO2; 95.0% N2, 45-65% humidity) or in hermetic jars with an anaerobic sachet (Anaeropack;
146 Thermo Fisher).

147 *Staining assays on MBEC biofilm plates*

148 Total biofilm biomass was evaluated using Gram's safranin-O solution (Sigma-Aldrich),
149 biofilm matrix-associated glycoproteins content using fluorescein wheat germ agglutinin
150 (WGA, 1/100 diluted, ThermoFisher), and viability using a resazurin assay (1 mg/ml; Sigma-
151 Aldrich)[15-17]. While WGA has specific affinity for sialic acid (SA) and N-acetylglucosamine
152 (NAG), we used it to assess the presence of matrix-associated glycoproteins containing these
153 sugar moieties (SA/NAG-glycoproteins). The dispersal rate was estimated at 24h by measuring
154 the ratio of viable biofilm-dispersed bacteria to total biofilm biomass. Briefly, MBEC were
155 transferred to 96 well plate containing stains and incubated at 37°C for 2 h (resazurin and
156 WGA) or 20' (safranin-O). Stains were recovered by sonication at 45 kHz (USC-500T, VWR) in
157 a plate containing acetic acid (30%, safranin-O) or 1.5M sodium chloride (WGA). Specific
158 absorbance (safranin-O) or fluorescence (WGA and resazurin) was measured using an EnSight
159 spectrophotometer (Perkin Elmer, Villepinte, France). An average of at least 12 biofilm
160 replicates were performed for each individual. A positive control was included for each
161 experiment (*E. Coli* LF82, a high biofilm producer).

162 *Donor fecal microbiota preparation*

163 Feces obtained from SWISS aged mice were divided into three groups of interest: young
164 (n=8 mice, 4 males and 4 females, 6 months old), aged robust (n=8 mice, 5 males and 3
165 females, 24 months old), and aged prefrail (n=8 mice, 5 males and 3 females, 24 months
166 old[13]). Feces were pooled in 1.5 mL phosphate buffered saline (PBS, Eurobio Scientific, Les
167 Ulis, France), homogenized, and filtered through a sterile nylon mesh strainer. The filtered

168 contents were centrifuged twice, and the pellet was resuspended in PBS/20% glycerol at
169 OD_{600nm}=1.5 (≈10^9 CFU/ml). All the procedures were performed under anaerobic conditions
170 at 37°C in an anaerobic chamber (Don Whitley A20).

171 *Post-antibiotics fecal microbiota inoculation*

172 C57BL/6 mice (Janvier, Le Genest Saint-Isle, France), aged 8 weeks, were housed under
173 specific pathogen-free conditions (CREFRE U006, CHU Purpan). Mice were divided into four
174 groups: 6M (gavaged with pooled 6-month-old microbiota, n=9), 24M robust (gavaged with
175 pooled 24-month-old microbiota, n=8), 24M prefrail (gavaged with pooled 24-month-old
176 microbiota, n=7), and a control group receiving PBS vehicle without microbiota (n=5). Animals
177 were housed in large cages (for rats) (maximum to 10 mice per cage) and acclimatized for 2
178 weeks. To control for coprophagy and potential cage effects, every two days cage bedding –
179 including cotton nests – was thoroughly mixed every two days by a single experimenter using
180 the same gloves throughout the procedure. After acclimatization phase, mice were
181 distributed across four cages (PBS vehicle, 6M, 24M-robust and 24M-prefrail). The existing
182 microbiota was perturbed by broad-spectrum antibiotics in drinking water at concentrations
183 of 1 g/l (ampicillin and metronidazole, Sigma-Aldrich) and 0.5 g/l (neomycin and vancomycin,
184 Sigma-Aldrich) for the first five days, and half-diluted for the remaining days. Given this
185 standardized mixing and group distribution, we collected fecal pellets from five randomly
186 selected animals during the acclimatization period and after antibiotic exposure. On day 10,
187 the mice underwent fecal microbiota inoculation via oral gavage with 200 µL of previously
188 described fecal slurry. Four days post-inoculation, the colon was harvested for evaluation of
189 macroscopic damage, including colon thickness edema (in mm) and blind Wallace scoring
190 endpoints[22], was assessed by a blinded and skilled experimenter. Animal procedures were

191 approved by the National Laboratory Animal Ethics Committee (APAFIS 2023060610225611,
192 French Ministry of Research).

193 *16S rRNA V3/V4 gene sequencing*

194 Total DNA was extracted from feces or biofilms using the EZNA isolation kit stool DNA
195 (VWR for biofilms) according to the manufacturer's protocol. DNA extraction and specific PCR
196 amplification of 16S bacterial rDNA V3-V4 regions were targeted by 341f-806R primers and
197 sequenced on the Illumina MiSeq 2 × 250 bp technology at Vaiomer (Toulouse, France) or
198 Biomnigene (Besancon, France). Demultiplexed raw read sequences were processed using
199 FROGS bioinformatics pipeline (FROGS v. 4.1.0[23], Galaxy Toulouse server, GenoToul). Adaptor
200 and primer sequences were trimmed, and amplicons were merged using Vsearch plugin
201 (v.2.17.0). Sequences were processed using swarm v2.0 for cluster filtering and denoising to
202 identify amplicon sequence variants (ASVs), with a 0.005% abundance threshold. The ASV
203 table was filtered using three criteria: minimum count of 4, 10% prevalence, and 10%
204 variance. No rarefaction, scaling, or transformation was applied to the data. Taxonomic
205 assignments were performed using the 16S SILVA 138.1 database.

206 *16S Fluorescent In situ hybridization (FISH)*

207 For fluorescence in situ hybridization (FISH), methacarn-fixed mouse colon tissues were
208 embedded in paraffin. Slides were hybridized with a universal bacterial 16S fluorescent rRNA
209 probe (EUB338-Cy3, 5'GCTGCCTCCCGTAGGAGT-Cy5, Eurofins Scientific, France) and DNA was
210 counterstained with 4',6-diamidino-2-phenylindole (DAPI, Invitrogen) and polysaccharide
211 content (wheat germ agglutinin labeled with fluorescein, ThermoFisher)[16,17]. The biofilm
212 damage score was blindly evaluated in at least three microscopic fields for each mouse in the
213 groups of interest, according to the criteria described in[17]. Briefly, the score was established
214 on five criteria: mucus layer invasion, bacterial-epithelial distance, biofilm density, bacterial

215 translocation, and cell presence in the lumen. Each parameter was scored 0-3, with higher
216 scores indicating greater mucosal biofilm disruption. Samples that were unsatisfactorily fixed
217 for scoring were excluded from analysis. Images were acquired using a Leica LSM 710 confocal
218 microscope (TRI Genotoul, Purpan), and FIJI freeware was used for the final image mounting
219 (v.1.51, Mac Os).

220 *Human intestinal epithelial cells*

221 Caco-2 (ATCC, Manassas, USA) and HT29-MTX E12 (ATCC) were grown separately in
222 Dulbecco's modified Eagle medium (DMEM, Eurobio Scientific, Les Ulis, France)
223 supplemented with 10% fetal bovine serum (FBS, Sigma-Aldrich), penicillin/streptomycin
224 (Invitrogen, Massy, France) and non-essential amino acid solution (Thermofisher, Paisley, UK)
225 at 37°C in a humidified incubator with 5% CO2 as previously described [24]. Coculture at 3:1
226 (Caco-2:HT29) was done on flat bottom 24-wells plates at an initial total density of 2.10^5 cell
227 per well (Corning, Thermo Scientific). Cells were screened for mycoplasma infection
228 (MycoAlertTM, Lonza, Bâle, Switzerland) and treated before coculture if necessary
229 (PlasmocureTM, Lonza). Cells were cocultured with dispersed bacteria from biofilms
230 (normalized optical density; OD_{600nm}=0.01) in OPTIMEM (Thermo Fisher). Bacterial adhesion
231 to the intestinal epithelium was assessed after 4 h of coculture on a blood agar plate[16,17].

232 *Relative mRNA expression by qRT-PCR*

233 Total RNA was extracted using TRIzol reagent (Euromedex, France) after 4 h of coculture
234 (Qiagen, Montreal, Canada). Reverse transcription of isolated RNA was performed using the
235 Maxima First Strand Kit (Invitrogen, Thermo Scientific) according to the manufacturer's
236 instructions. Quantitative PCR (RT^2qPCR Primer, Qiagen) was performed on a LightCycler
237 (Roche, Basel, Switzerland) based on SYBR Green technology, using the Takyon Low Rox SYBR
238 kit (Eurogentec, Seraing, Belgium). Data were analyzed by the $2^{-\Delta\Delta CT}$ method using HPRT and

239 GAPDH (Qiagen) as control genes and expressed as fold change compared to control cells
240 without bacteria. PCR primers used in this study are listed in Supplementary Table 9.

241 *Grape pomace intervention*

242 After maturation, MBEC Assay® was exposed to grape pomace solution diluted in
243 microbiological BHI supplemented broth at several concentrations (0.3 to 30 mg/mL) for 24h.
244 The medium was refreshed, and 4h later dispersed bacteria were collected to collect biofilm-
245 dispersed bacteria for interaction assays with human intestinal epithelial cells. Staining assays
246 were performed in parallel to estimate the effect of grape pomace on biofilm biomass and
247 matrix-associated glycoproteins content. The industrial grape pomace used (VinOgrape™,
248 Nexira, France) was an extract containing purified polyphenols (>90% content, quantified by
249 spectrophotometry method) anthocyanins, catechin, epicatechin and oligomeric
250 proanthocyanidins.

251 *Statistics and visualization*

252 We performed statistical analyses and data visualization using R 4.3.0 – Posit (Rstudio IDE)
253 v2023.0.9.1 built 494 (Posit Team 2023, Boston, MA, USA) and GraphPad Prism (v10 for
254 MacOs, La Jolla, USA). Baseline clinical characteristics were compared between the groups
255 with chi-squared test for categorical variables and ANOVA (Fisher test) for continuous
256 variables with Tukey's method to correct P-values. To explore the bacterial taxonomy
257 variability among sample groups, alpha and beta diversity metrics were performed in R using
258 phyloseq (v.1.46.0). Principal coordinate analysis (PCoA) and Partial least squares-
259 discriminant analysis (PLS-DA) and principal component analysis (PCA) were performed in R
260 using phyloseq (v. 1.46.0), mixomics (v. 6.26) and compared using PERMANOVA
261 (pairwiseAdonis v.0.4.1) with 9999 permutations. To calculate microbiome uniqueness—a
262 novel metric introduced in the context of age-related microbiome alterations[25]—we averaged

263 the lowest beta diversity values for each individual across multiple distance metrics, including
264 Bray-Curtis, Jaccard, unweighted UniFrac, and weighted UniFrac, compared to all other
265 individuals within the same experimental group. This metric quantifies how distinct each
266 individual's microbiome is from its nearest neighbor within the cohort, with higher values
267 indicating greater compositional distinctness. Rarefaction curves (Supplementary Figure 1A)
268 and taxa bar plots were generated in R using phyloseq (v. 1.46.0) and ggnested (v. 0.1.0).
269 Statistical differences between microbial communities were assessed in R using LEfSe (lefser
270 v.1.12[26]), Deseq2 (v.1.42[27]), EdgeR (v.4.0.3[28]), metagenomeSeq (v.1.43.0[29], and ANCOM[30].
271 Boxplots, barplots and scatter plots were generated in R using ggplot2 (v.3.4.4) and ggpubr
272 (v.0.6.0). Heatmaps were created in R using complexheatmap (v.2.18.0). Grout's test was
273 used to filter statistical outliers in the qPCR dataset (GraphPad Prism). Statistical significance
274 was set at $P < 0.05$. For group comparisons, we used Dunnett's or Tukey's method to correct
275 P-values for ANOVA and the Benjamini-Hochberg method for differential abundant taxa
276 analyses. Unless otherwise indicated, values are presented as the mean ± standard error of
277 the mean.

278 **3. RESULTS**

279 **Characterization of the human cohort**

280 Samples were collected from 42 individuals, stratified into 13 healthy individuals aged 30-
281 70 years and 29 individuals aged ≥ 70 years. Within the aged group, 15 were robust based on
282 the Fried frailty index[2], while 14 were prefrail (score of 1 and 2) (Table 1 and Supplementary
283 Table 1). All the donors had satisfactory nutritional scores (Supplementary Table 3). As
284 expected, the Charlson comorbidity index [19] indicated more comorbidities in aged individuals
285 than in younger donors (0.923±1.19 versus 4.73±1.87, $P<0.001$), but this index was not

286 discriminant between prefrail and robust donors (5.07±1.59 versus 4.73±1.87, p=0.836;
287 Supplementary Table 6). General characteristics of donors used in the study are summarized
288 in Table 1.

289 **Taxonomic characterization of microb-aging on human biofilms**

290 To explore links between microb-aging and prefrailty syndrome, we cultured the fecal
291 microbiota of aged individuals on a mucin-coated device, in an attempt to reproduce a
292 mucosal polymicrobial anaerobic biofilm[14,16,17]. Despite a decline in Bacteroidota (formerly
293 Bacteroidetes) compared to fecal sample, biofilm communities remained dominated by
294 Bacillota (formerly Firmicutes), specifically *Ruminococcaceae*, *Christensenellaceae*,
295 *Bifidobacteriaceae*, *Akkermansiaceae*, *Lachnospiraceae*, and *Oscillospiraceae* (Figure 1A,
296 Supplementary Figure 1). These taxa are core members typically found in human fecal
297 microbiota (Supplementary Figure 2). The *ex vivo* biofilm model did not show statistically
298 significant differences in α-diversity compared to 30-70 years individuals (Supplementary
299 Figure 1C). Regarding β-diversity on weighted Unifrance distance, the groups were not
300 statistically separated (PERMANOVA >0.05, Supplementary Figure 1D). However, we
301 observed that biofilms from aged robust donors exhibited greater individual microbiome
302 uniqueness compared to those from prefrail donors (Figure 1B). We ran various statistical
303 models in metagenomics to identify differentially abundant taxa (i.e., Deseq2,
304 metagenomeSeq, ANCOM, and edgeR, Supplementary Tables 10 and 11). We found
305 correspondence in age-related taxa abundance between the biofilm model and other reports
306 on human aging cohorts[5-8] (Supplementary Figures 1E-F). Specifically, aged individuals
307 presented an enrichment of taxa including *Selemonadaceae*, *Prevotellaceae*, and potential
308 pathobionts such as *Enterobacteriaceae*. Concomitantly, there was a reduction in the
309 abundance of important commensals within aged biofilms, including *Dialister sp.,*

310 *Akkermansia sp.* and *Bifidobacteriaceae* (Supplementary Figure 1E). Biofilms from aged
311 robust individuals displayed a higher abundance of *Prevotellaceae* compared to prefrail
312 individuals, as well as an increased representation of *Selenomonadaceae (Megamonas sp.)*
313 and *Ruminococcaceae* (Supplementary Figure 1F).

314 We then expanded the investigation between clinical characteristics of donors and taxa
315 abundance in the biofilm model. We identified 34 statistically significant correlation pairs with
316 biofilm taxonomic features and clinical characteristics, primarily at the Family and Genus
317 levels (Figure 1C). First, aging alone was linked to a diminished abundance of core taxa such
318 as *Slackia sp.*, *Eggerthellaceae*, and Bifidobacteriales. In addition, we found a positive
319 correlation between prefrailty and the relative abundance of *Monogobales, Oscillibacter sp.*
320 and *Negativibacillus sp* (Figure 1C). Regarding clinical history, the Charlson comorbidity index
321 was negatively correlated with abundance of *Slackia sp*., and *Veillonellaceae (Dialister sp.)*.
322 Abundances of *Pasteurellaceae* and *Haemophilus sp.* were inversely correlated with the MNA
323 score, shedding light on the potential links between these specific taxa and nutritional status
324 (Figure 1C). Gender exhibited no statistically significant correlation with the abundance of
325 microbial taxa in cultured biofilms (Figure 1C). Finally, regarding the living conditions of
326 donors, we uncovered a positive correlation between conjugal lifestyle and the microbial
327 abundance of several taxa, including *Tannerellaceae*, *Parabacteroides sp.*, and *Butyricimonas*
328 *sp.* (Figure 1C). Altogether, these data indicate that several microbial signatures associated
329 with aging and prefrailty are preserved in this biofilm model.

330 **Physical structure of human biofilms is altered in prefrail donors**

331 To explore microb-aging beyond taxonomy, we first characterized the physical structure
332 of biofilms. We observed a negative correlation between donor age and total biofilm biomass
333 (Pearson R = -0.6, P<0.05, Figure 2A). However, this feature was not significantly different

334 between prefrail and robust biofilms (Figure 2B). Regarding the extracellular matrix of
335 biofilms, we found a positive correlation (R=0.39, P<0.05) between age and proportion of
336 SA/NAG-glycoproteins within this matrix (Figure 2D). Interestingly, biofilms from prefrail
337 donors exhibited a heightened glycoproteins matrix composition compared to the other
338 samples (Figure 2E). We then investigated the links between the clinical characteristics of
339 human donors and biofilm physical structure (Kendall's correlation approach, Figure 2C). In
340 addition to confirming the previously described Fried and age relationship, we found a
341 negative correlation between biofilm biomass and the Charlson comorbidity index (Figure
342 2C). Neither the donor's sex, household, nor diet (MNAscore) demonstrated a significant
343 association with the biofilm structure (Figure 2C). Focusing on biofilm taxonomy (Figure 2F),
344 we identified that high biomass biofilm, a feature of 30-70 yrs biofilms, was positively
345 correlated with a high abundance of *Eggerthellaceae*, *Oscillospira sp.*, *Enterorhabdus sp.*, and
346 *Slackia sp.* High biofilm matrix- SA/NAG-glycoproteins, a feature of prefrail biofilms, was
347 correlated with donors harboring low abundance of Coriobacteriales and *Eggerthellaceae*
348 (Figure 2F). Overall, these observations suggest that the physical structure of biofilms
349 generated from 30-70 and aged individuals differs and, more importantly, that these physical
350 modifications may serve as discriminant features between aged individuals predisposed to
351 prefrailty or robustness.

352 **Prefrailty-associated human biofilms have an hypervirulent phenotype**

353 In addition to the physical structure, we evaluated the pathogenic behavior of human
354 biofilms between young and aged donors. First, we assessed the stability of biofilms,
355 measured as the rate of bacterial dispersal over a 24-hour period. High dispersal is considered
356 a virulent trait that increases the likelihood of exposing the subjacent host epithelium to
357 unwanted bacterial contact [15,16]. Donor age was not statistically correlated with this feature

358 (P=0.058, Figure 3A). However, prefrail biofilms had a significantly higher dispersal rate than
359 biofilms from younger groups (P<0.05, Figure 3B). We then explored the ability of biofilms to
360 disperse bacteria that could attach to the underlying intestinal epithelium. To this end, we
361 exposed enterocyte/mucus-producing human epithelial cell lines to a normalized
362 concentration of the dispersed biofilm bacteria. We found that higher chronological age
363 correlated with this behavior (P<0.05, Figure 3D). More importantly, it was dispersed bacteria
364 from prefrail biofilms that exhibited heightened adhesiveness compared to other groups
365 (P<0.01, Figure 3E). Intriguingly, the adhesiveness of bacteria was correlated with individuals
366 having a high Charlson comorbidity index, suggesting a potential connection between
367 bacterial behavior and clinical history (Figure 3C). In this cohort, neither the donor's gender,
368 household, nor diet (MNA score) demonstrated a statistically significant correlation's index
369 with biofilm pathogenic behavior (Figure 3C). Regarding taxonomy, biofilm dispersal was
370 statistically correlated with a lower abundance of *Ruminococcaceae* and *Oscillospirales sp*. In
371 addition, we identified several taxa whose abundance was either positively (e.g.,
372 *Adlercreutzia sp.* and Coriobacteriales) or negatively (e.g., *Akkermansiaceae*) correlated with
373 biofilm bacterial adhesiveness (Figure 3F). In summary, our findings underscore that while
374 chronological age plays a limited role in influencing biofilm behaviors, prefrailty status
375 emerges as a key factor shaping the instability and virulence of gut biofilms.

376 **Prefrailty-associated biofilms trigger host innate response in human intestinal**
377 **epithelium**

378 We then focused on the relative expression of 10 genes encoding proinflammatory
379 cytokines, antimicrobials, and tight junction proteins to discern patterns indicative of the host
380 epithelial innate response to these biofilm-dispersed bacteria. The scaled expression
381 heatmap revealed not only altered expression patterns in biofilms from aged versus younger

382 individuals, but also striking disparities within biofilms from prefrail versus robust individuals
383 (Figure 4A). Proinflammatory genes, such as *IL6* and *TNF*, and the tight junction genes claudin-
384 2 (*CLDN2*) and occludin (*OCLN*) (Figure 4B) exhibited a notable trend towards increased
385 expression in prefrail versus robust individuals. While such trends failed to reach statistical
386 significance when considered alone – except in the case of *TNF* and *IL6* – the PCA ordination
387 plot demonstrated a clear shift in the transcriptome of epithelia exposed to bacteria from
388 prefrail individuals compared to younger individuals (Figure 4C, PERMANOVA P= 0.007). As
389 visualized in the biplot vectors, genes with the greatest contribution in the separation were
390 those coding for proinflammatory signals (*TNF*, *IL8 and IL6* along the PC1 axis) and those
391 related to tight junction proteins (*CLDN2* and *OCLN* in the PC2 axis). Expanding this analysis
392 with biofilm features, we discovered that high dispersal rate – indicative of a virulent prefrail
393 phenotype – was correlated with a higher expression of inflammatory genes (*IL6* and *TNF*,
394 Figure 4D). Interestingly, high adhesiveness was also positively correlated with inflammatory
395 genes (*COX2*) as well as genes encoding tight junction proteins (*CLDN2* and *OCLDN*; Figure
396 4C). Finally, we found that an increased quantity of SA/NAG-glycoproteins in the biofilm
397 matrix – a feature linked to aging and prefrailty – was positively correlated with a higher
398 expression of proinflammatory genes (*IL6*, *IL8*, and *TNF*). Overall, these findings indicate that
399 in addition to aging host immunity, microbiota biofilms from +70 years prefrail individuals,
400 but not in 30-70 years and +70 years robust individuals, contain commensals with
401 proinflammatory triggering potential.

402 **Prefrailty aging in mice is linked to altered mucosal biofilm biogeography in colon.**

403 Motivated by human biofilm model findings, we aimed to confirm whether early signs of
404 prefrailty could influence the spatial organization of the gut microbiota in the colon. For this,
405 we used tissues from an aging mouse cohort, equivalent to humans aged 30 to 70+ years (= 6

406 to 24 months old, INSPIRE mouse cohort[13]). Among the 15 selected animals, thorough frailty
407 syndrome assessments were conducted, categorizing them into groups mirroring healthy
408 aging (robust, n=8) and those displaying early signs of frailty (prefrail, n=7, Valencia Frailty
409 Score, Supplementary Table 8[20]). Upon sacrifice, the colon-associated microbiota was
410 visualized using 16S fluorescent *in situ* hybridization (FISH) staining (Figures 5 A-C).
411 Remarkably, young mice exhibited a mucosal microbiota organized as a dense biofilm
412 community lining a layer of sterile mucus (outlined by dashed lines in yellow, Figure 5A). In
413 contrast, aged animals displayed a different spatial organization, featuring isolated bacteria
414 within the mucus layer that escaped from the dense mucosal biofilm (arrows, Figures 5B and
415 5C). Bacterial translocation, which was almost absent in the young cohort, was observed in
416 the aged animals (Figures 5B and 5C). Notably, aged prefrail animals exhibited more signs of
417 tissue-associated biofilm alterations than aged robust animals, including signs of virulent
418 behavior in gut microbiota such as invasion of the mucus sterile layer, epithelial adhesion, or
419 translocation (biofilm damage score[17], Figure 5D). These findings confirmed *in vivo* that
420 prefrail status in aging is linked to altered biofilm organization and emergence of virulent
421 phenotypes.

422 **Prefrailty-associated microbiota directly causes colon damage when inoculated into**
423 **young mice**

424 To experimentally demonstrate a causal relationship between prefrailty-associated
425 microbiota and local gut inflammation, we orally inoculated fecal microbiota in antibiotic-
426 treated young mice. We used as inoculate a pool of feces from young (6 months, n=8), robust
427 (24 months, n=8), and prefrail mice (24 months, n=8). As expected, the antibiotic regimen
428 caused taxonomic dysbiosis in gut microbiota, with severe reduction of total load, alpha
429 diversity, and an increased abundance of *Enterobacteriaceae*, which was partially restored

430 after 4 days of antibiotic washout (Figure 5E, Supplementary Figures 3-5). Post-inoculation,
431 animals were monitored daily for 4 days, and no animals reached a distress endpoint
432 (Supplementary Figure 6A). Mice inoculated with prefrail microbiota exhibited a significant
433 difference in beta-diversity compared to those receiving aged robust or young microbiota
434 (Supplementary Figure 4D). Furthermore, we observed a higher abundance of Proteobacteria,
435 and a reduced abundance of *Muribaculaceae*, *Christensenellaceae*, *Parabacteroides* sp., and
436 *Akkermansia* sp., in mice inoculated with prefrail microbiota compared to the other groups,
437 mirroring previous findings in the litterature[31] (Supplementary Figure 5). Regarding intestinal
438 tissue damage after the inoculation procedure, we found that young fecal microbiota did not
439 cause macroscopic harm in the colon (total damage score of 1.7±0.44, Figure 5F-G,
440 Supplementary Figure 6B). When inoculated with aged prefrail microbiota, recipient animals
441 had significantly higher colon damage such as increased incidence of erythema, mucus
442 release in the lumen, edema, and (total score 5.4±0.98, ANOVA followed by Dunnett's test, P
443 = 0.002, Figure 5G). Additional histological analysis on these mice using FISH staining showed
444 reduced bacteria-epithelium distance in prefrail mice compared to young mice (but not
445 compared to aged-robusts), indicating a potentially compromised colonic barrier integrity in
446 the prefrail group (Supplementary Figure 6C). These results combined with previous *in vitro*
447 assays on intestinal epithelial cell lines, suggest that microbiota from prefrail – but not from
448 young and robust – may directly causes intestinal damage when inoculated into recipient
449 young mice.

450 **Grape pomace partially reverses prefrailty-associated biofilm structure and virulence**

451 Considering the virulent phenotype of the prefrail microbiota and its associated damage
452 to the intestinal mucosa, we investigated whether this phenotype can be reversed by
453 microbiota-targeted strategies. Grape-derived polyphenols have demonstrated prebiotic

454 properties via their activities on gut microbes[32-35]. Indeed, the majority of edible grape
455 polyphenols are poorly bioavailable and reach the colonic compartment where they shape
456 microbiome profile[36]. Therefore, we sought to determine whether industrial grape pomace,
457 which is already marketed as a food supplement in France, can affect the structure and
458 virulence of mucosal biofilms associated with prefrail aging. We previously observed that
459 prefrail biofilms had reduced biomass compared to young biofilms, and exposure to grape
460 pomace significantly increased it (Figure 6A, $P<0.05$ at 30 mg/ml). Importantly, we found a
461 statistically significant reduction of 79.5% in the dispersal rate in prefrail biofilms (Figure 6B,
462 $P<0.05$ at 30 mg/ml). However, grape pomace had no significant effect on the increased
463 adhesiveness of dispersed bacteria from prefrail biofilms (Figure 6C). At a concentration of 30
464 mg/ml, biofilm exposure to grape pomace led to a significant reduction of dispersed bacteria
465 able to trigger the expression of *IL6* (55% reduction, $P<0.05$, Figure 6D), while having no
466 statistically significant impact on levels of *IL8* and *TNF* ($P>0.05$, Figure 6E-F). Overall, these
467 experiments using a biofilm model suggested that grape pomace could directly reduce the
468 hypervirulent phenotype associated with the prefrail aging microbiota.

469 **4. DISCUSSION**

470 Aging is commonly associated with changes in the gut microbiota, including shifts in
471 taxonomy and metabolism, a phenomenon referred to as microb-aging [6]. Despite extensive
472 research on fecal microbiome from various populations worldwide (reviewed in[5-8]), significant
473 knowledge gaps remain on the ecological implications of microb-aging within commensal gut
474 communities. Another under-explored area is the causal relationship between microb-aging
475 and low-grade inflammation of aging [9,37]. Additionally, the role of microbiota in frailty aging
476 and the potential of microbiota-targeted therapies in transitioning from prefrailty to

477 robustness remain open questions. Addressing these gaps is crucial for understanding the
478 nature of microb-aging and identifying non-chronological markers of unhealthy aging [4,11].
479 Using non-invasive samples in a clinically well characterized human aging cohort, we thus
480 aimed at generating a model for microbiota forming biofilm, which is the microbial lifestyle
481 that resides in close proximity to the host tissue and epithelium [14]. In this study, we aimed at
482 detecting microbiome shifts in biofilms from aged individuals at an early stage of frailty,
483 including but not limited to taxonomy, specifically to uncover potential therapeutic
484 interventions that can reverse these changes and establish new targets that promote the
485 transition from prefrailty to robustness [10].

486 From a taxonomic perspective, the cultured biofilm maintained important microb-aging
487 features already described in the literature, such as increased microbiome uniqueness in
488 robust but not in prefrail aged individuals (Figure 1B)[25]. By comparing biofilm taxonomy
489 results with a recent grouping proposed by Ghosh et al.[5] — Groups I, II, and III—we observed
490 an interesting parallelism, where gut pathobionts, such as Proteobacteria from the
491 *Enterobacteriaceae* family, exhibited increased abundance in aged individuals. We also noted
492 a decline of beneficial taxa in aged biofilms, such as *Bifidobacteriaceae*. Interestingly,
493 *Akkermansia sp.*, a genus containing important commensals involved in host/mucus
494 homeostasis[38], showed slightly reduced abundance in aged biofilms. Intriguingly, biofilms
495 from aged robust individuals displayed increased taxa traditionally associated with cohorts of
496 healthy centenarians such as *Christencellaneaceae* [39-41]. As a limitation of these taxonomy
497 findings relates to small sample size, further investigation within the entire INSPIRE cohort
498 could be engaged to confirm and refine the identified taxonomic features (+1000
499 volunteers[12]). In addition, the longitudinal design of this cohort will enable collection from
500 the same individuals over the next 10 years, enabling us to track the progression of prefrailty

501 in individuals and determine whether they experience a shift to frailty, provided that microb-
502 aging is not therapeutically managed (with diet, exercise or pre- and probiotics).
503 In addition to taxonomic alterations, this study revealed new microbiological features that
504 may help distinguish between healthy and unhealthy aging in humans. Specifically, we
505 identified a reduced biofilm-forming capacity in most fecal samples of aged individuals
506 compared to that in younger individuals (Figure 2). This may indicate a common biological
507 pattern in the aging microbiome that is potentially linked to the loss or gain of specific taxa,
508 as previously discussed. More compelling are those features that distinguish between aged-
509 matched robust and prefrail donors, such as the amount of sialic acid/N-acetylglucosamine--
510 rich glycoproteins associated with the biofilm matrix (Figure 2). Extracellular polysaccharides
511 are indeed fundamental for retaining water within the biofilm matrix, generating a highly
512 hydrated and cohesive environment that influences cell movement [42,43]. Whether the altered
513 glycoproteins composition of the aged prefrail biofilms used in the present study contributes
514 to taxonomic changes, increased dispersal, and fragmented biofilm physical structure *in vitro*
515 (Figure 3) and *in vivo* (Figure 5) remains to be experimentally elucidated. Another discriminant
516 feature of prefrailty-associated biofilms is their capacity to release bacteria with higher
517 adhesiveness and which triggers proinflammatory signals from the underlying epithelium
518 (Figure 4). Although this phenomenon has not been previously documented, metagenomic
519 studies of fecal microbiota have indicated an increased proportion of virulence gene
520 pathways in microbiota from aged frail individuals [44].
521 It is yet to be fully understood whether local gut microbiota alterations directly contribute
522 to adverse outcomes in aged frail populations. Complementing *in vitro* findings, an *in vivo*
523 microbiota inoculation approach reinforces the hypothesis that prefrailty associated
524 microbes could directly cause a sub-inflammatory phenotype in the gut. Although this aligns

525 with other studies of aged microbiota transfer [45], the novel message from the present study
526 lies in the separation between robustness and prefrailty-associated sampling. Here, we found
527 that macroscopic colon damage induced by aged microbiota may be more pronounced with
528 prefrail microbiota than with robust (Figure 5G). Undoubtedly, the interaction between the
529 gut microbiome and its host is bidirectional and more complex links are expected *in vivo*. A
530 road to be explored is the impact of a prefrailty microbiota within an aging host, where
531 heightened inflammatory stress and immunosenescence may compromise the host's ability
532 to mount an effective response to local insults (the inflammaging hypothesis [37]). In addition
533 to the virulent behavior of prefrail biofilm, local inflammation may significantly alter microbial
534 biotope making it less favorable to commensal gut bacteria, or even promoting the blooming
535 of pathogenic taxa (e.g., *Enterobacteriaceae* [46]). This could be attributed to compromised
536 epithelial secretory functions in high age, such as defective mucus and antimicrobial peptide
537 production[47], or deficiencies in intestinal barrier integrity [48]– although the latter phenomenon
538 remains a subject of debate [49]. Natural polyphenols, including those present in grape pomace,
539 have been shown to improve cognitive function, extend the lifespan, and protect against age-
540 related muscle loss in several mice models [32-35]. Studies in mice have shown that grape
541 pomace in the diet can improve metabolic diseases by preventing gut microbiota dysbiosis
542 and increasing the abundance of beneficial taxa [50-52]. In this study, we found that an industrial
543 grape pomace preparation favored the restoration of the physical and non-pathogenic
544 features of prefrail biofilms *in vitro*, potentially indicating the improved resilience of microb-
545 aging communities (Figure 6). Additionally, this compound reduced the release of
546 proinflammatory triggering bacteria from prefrail biofilms. Previous study suggested that
547 grape pomace did not cause a significant taxonomic shift in human gut microbiota [53].
548 Therefore, further research is needed to determine the precise impact of grape polyphenols

549 on microbial virulence functions and to elucidate specific microbial genetic responses. Finally,
550 going beyond this particular compound, the methodology presented here may support the
551 clinical relevance of gut microbiota biofilm cultures (using non-invasive fecal samples) to
552 assess and validate the effects of new classes of geroprotectors, such as prebiotics or
553 probiotics, specifically targeting signs of unhealthy microb-aging.

554 Beyond the well-known taxonomic changes in the aging gut microbiome, this study points
555 to novel functional and behavioral changes in human gut biofilm, that switched to a virulent
556 phenotype in prefrail individuals but not in robusts. Importantly, we found that this
557 phenotype was reversible by polyphenol-rich grape pomace treatment. Altogether, these
558 results further establish the intestinal microbiota as a target to improve healthy aging. These
559 discoveries might represent a unique opportunity for geroclinicians to develop screening
560 tools and identify new therapeutic targets against microb-aging, to prevent frailty
561 development in the expanding aging population.

562 **Author Contributions:** GLC. performed most experiments, analyzed data, and provided
563 clinical input; MP., EM., JT., EP., CD., NV. and JPM. contributed to *in vivo* and *in vitro* data
564 acquisition and analysis; SG., and BV. provided human samples, contributed to clinical
565 characterization, and reviewed manuscript; YS., BG., and A.P provided mice samples,
566 contributed to clinical characterization and reviewed manuscript; LB., BB. reviewed
567 manuscript and provided clinical input; DG. provided scientific reagents and reviewed the
568 manuscript; JPM. performed 16S bioinformatics and statistics; GLC., NV. and JPM., wrote the
569 manuscript; N.V and JPM. supervised the work and obtained fundings. All authors have read
570 and agreed the final version of the manuscript.

571 **Data Availability:** 16S rRNA gene sequencing from the experimental biofilms and mouse
572 data were uploaded to the NCBI Sequence Read Archive (SRA Bioproject PRJNA1076354).
573 Additional biological or clinical metadata from the INSPIRE-T cohort can be obtained by
574 contacting the corresponding author, who will submit the request to the INSPIRE biobanking
575 and research committee for final approval. Other information from this study can be
576 obtained, upon reasonable requests, from the corresponding author.

577 **Ethics:** The INSPIRE cohort protocol ID NCT04224038 was approved by the French Ethical
578 Committee located in Rennes (CPP Ouest V) in October 2019. Mice experimentation protocol
579 has been approved by local ethic committee of Toulouse University and by the Ministry of
580 Superior Education and Research under the agreement APAFIS2023060610225611.

581 **Acknowledgments:** Authors thank the Department of Gastroenterology and
582 Pancreatology at the University Hospital of Toulouse for an MD/PhD scholarship leave to GLC.
583 Authors give credit to Dr. Felipe Sierra for its initial assessment of the research project, under
584 the umbrella of INSPIRE Call for Geroscience Research Grant. Authors thank the INSPIRE
585 biobanking committee for evaluating our project and approving sample collection. Authors

586 thank the staff of the human and mice Centre de Recherche Biologique (CRB) of the Toulouse
587 Hospital for samples preparation. Authors thank the CREFFRE core facility (UMS 006) for
588 hosting animals used in the project and contributing to histopathology analyses (R. Balouzat
589 and S. Milia), and the TRI-Genotoul platform for cellular imaging facilities (U1043, S. Allart).
590 Authors are thankful to Dr. Racaud-Sultan for critically reading the manuscript. Fundings came
591 from INSPIRE-Grant AMIGO / ANR dysBIOFILM ANR-22-CE14-0041-01 (JPM), ANR-PARCURE
592 PRCE-CE18, 2020 (NV), and the national program "Microbiote" from INSERM (NV and JPM).
593 The INSPIRE-T study was supported by grants from the Region Occitanie/Pyrénées-
594 Méditerranée (Reference number: 1901175), the European Regional Development Fund
595 (ERDF) (Project number: MP0022856), and the Inspire Chairs of Excellence funded by:
596 Alzheimer Prevention in Occitania and Catalonia (APOC), EDENIS, KORIAN, Pfizer, Pierre-
597 Fabre. The IHU HealthAge Open Science initiative was supported by the French National
598 Research Agency (ANR) as part of the France 2030 program (ANR-23-IAHU-0011), and builds
599 on the work conducted in the Data Sharing Alzheimer project.

600 **Competing Interests:** Prebiotic product (grape pomace) was gratuitously furnished by the
601 NEXIRA company (Rouen, France) and covered by a collaborative research grant between DG.
602 and NV. The company acknowledges having no influence on the results obtained during
603 assays presented in this manuscript.

604 **References**

605 1 World Health, O. *Decade of healthy ageing: baseline report*. (World Health Organization,
606 2020).
607 2 Fried, L. P. *et al.* Frailty in older adults: evidence for a phenotype. *J Gerontol A Biol Sci Med*
608 *Sci* **56**, M146-156 (2001). https://doi.org/10.1093/gerona/56.3.m146
609 3 Romero-Ortuno, R. & Kenny, R. A. The frailty index in Europeans: association with age and
610 mortality. *Age Ageing* **41**, 684-689 (2012). https://doi.org/10.1093/ageing/afs051
611 4 Sierra, F. The Emergence of Geroscience as an Interdisciplinary Approach to the
612 Enhancement of Health Span and Life Span. *Cold Spring Harb Perspect Med* **6**, a025163 (2016).
613 https://doi.org/10.1101/cshperspect.a025163
614 5 Ghosh, T. S., Shanahan, F. & O'Toole, P. W. The gut microbiome as a modulator of healthy
615 ageing. *Nat Rev Gastroenterol Hepatol* **19**, 565-584 (2022). https://doi.org/10.1038/s41575-
616 022-00605-x
617 6 Bosco, N. & Noti, M. The aging gut microbiome and its impact on host immunity. *Genes*
618 *Immun* **22**, 289-303 (2021). https://doi.org/10.1038/s41435-021-00126-8
619 7 DeJong, E. N., Surette, M. G. & Bowdish, D. M. E. The Gut Microbiota and Unhealthy Aging:
620 Disentangling Cause from Consequence. *Cell Host Microbe* **28**, 180-189 (2020).
621 https://doi.org/10.1016/j.chom.2020.07.013
622 8 O'Toole, P. W. & Jeffery, I. B. Gut microbiota and aging. *Science* **350**, 1214-1215 (2015).
623 https://doi.org/10.1126/science.aac8469
624 9 Le Cosquer, G., Vergnolle, N. & Motta, J. P. Gut microb-aging and its relevance to frailty
625 aging. *Microbes Infect* **26**, 105309 (2024). https://doi.org/10.1016/j.micinf.2024.105309
626 10 Gill, T. M., Gahbauer, E. A., Allore, H. G. & Han, L. Transitions between frailty states among
627 community-living older persons. *Arch Intern Med* **166**, 418-423 (2006).
628 https://doi.org/10.1001/archinte.166.4.418
629 11 Ader, I. *et al.* Healthy Aging Biomarkers: The INSPIRE's Contribution. *J Frailty Aging* **10**, 313-
630 319 (2021). https://doi.org/10.14283/jfa.2021.15
631 12 de Souto Barreto, P. *et al.* The INSPIRE Research Initiative: A Program for GeroScience and
632 Healthy Aging Research Going from Animal Models to Humans and the Healthcare System. *J*
633 *Frailty Aging* **10**, 86-93 (2021). https://doi.org/10.14283/jfa.2020.18

634 13 Santin, Y. *et al.* Towards a Large-Scale Assessment of the Relationship between Biological
635 and Chronological Aging: The INSPIRE Mouse Cohort. *J Frailty Aging* **10**, 121-131 (2021).
636 https://doi.org/10.14283/jfa.2020.43
637 14 Motta, J. P., Wallace, J. L., Buret, A. G., Deraison, C. & Vergnolle, N. Gastrointestinal
638 biofilms in health and disease. *Nat Rev Gastroenterol Hepatol* **18**, 314-334 (2021).
639 https://doi.org/10.1038/s41575-020-00397-y
640 15 Motta, J. P. *et al.* Hydrogen sulfide protects from colitis and restores intestinal microbiota
641 biofilm and mucus production. *Inflamm Bowel Dis* **21**, 1006-1017 (2015).
642 https://doi.org/10.1097/MIB.0000000000000345
643 16 Motta, J. P. *et al.* Iron Sequestration in Microbiota Biofilms As A Novel Strategy for Treating
644 Inflammatory Bowel Disease. *Inflamm Bowel Dis* **24**, 1493-1502 (2018).
645 https://doi.org/10.1093/ibd/izy116
646 17 Motta, J. P. *et al.* Active thrombin produced by the intestinal epithelium controls mucosal
647 biofilms. *Nat Commun* **10**, 3224 (2019). https://doi.org/10.1038/s41467-019-11140-w
648 18 Rubenstein, L. Z., Harker, J. O., Salva, A., Guigoz, Y. & Vellas, B. Screening for undernutrition
649 in geriatric practice: developing the short-form mini-nutritional assessment (MNA-SF). *J*
650 *Gerontol A Biol Sci Med Sci* **56**, M366-372 (2001). https://doi.org/10.1093/gerona/56.6.m366
651 19 Charlson, M. E., Pompei, P., Ales, K. L. & MacKenzie, C. R. A new method of classifying
652 prognostic comorbidity in longitudinal studies: development and validation. *J Chronic Dis* **40**,
653 373-383 (1987). https://doi.org/10.1016/0021-9681(87)90171-8
654 20 Gomez-Cabrera, M. C. *et al.* A New Frailty Score for Experimental Animals Based on the
655 Clinical Phenotype: Inactivity as a Model of Frailty. *J Gerontol A Biol Sci Med Sci* **72**, 885-891
656 (2017). https://doi.org/10.1093/gerona/glw337
657 21 Dague, E. *et al.* Probing in vitro interactions between Lactococcus lactis and mucins using
658 AFM. *Langmuir* **26**, 11010-11017 (2010). https://doi.org/10.1021/la101862n
659 22 Wallace, J. L., Le, T., Carter, L., Appleyard, C. B. & Beck, P. L. Hapten-induced chronic colitis
660 in the rat: alternatives to trinitrobenzene sulfonic acid. *J Pharmacol Toxicol Methods* **33**, 237-
661 239 (1995). https://doi.org/10.1016/1056-8719(95)00001-x
662 23 Bernard, M., Rue, O., Mariadassou, M. & Pascal, G. FROGS: a powerful tool to analyse the
663 diversity of fungi with special management of internal transcribed spacers. *Brief Bioinform* **22**
664 (2021). https://doi.org/10.1093/bib/bbab318

665 24 Rolland-Fourcade, C. *et al.* Epithelial expression and function of trypsin-3 in irritable bowel
666 syndrome. *Gut* **66**, 1767-1778 (2017). https://doi.org/10.1136/gutjnl-2016-312094
667 25 Wilmanski, T. *et al.* Gut microbiome pattern reflects healthy ageing and predicts survival
668 in humans. *Nat Metab* **3**, 274-286 (2021). https://doi.org/10.1038/s42255-021-00348-0
669 26 Segata, N. *et al.* Metagenomic biomarker discovery and explanation. *Genome Biol* **12**, R60
670 (2011). https://doi.org/10.1186/gb-2011-12-6-r60
671 27 Love, M. I., Huber, W. & Anders, S. Moderated estimation of fold change and dispersion
672 for RNA-seq data with DESeq2. *Genome Biol* **15**, 550 (2014). https://doi.org/10.1186/s13059-
673 014-0550-8
674 28 Robinson, M. D., McCarthy, D. J. & Smyth, G. K. edgeR: a Bioconductor package for
675 differential expression analysis of digital gene expression data. *Bioinformatics* **26**, 139-140
676 (2010). https://doi.org/10.1093/bioinformatics/btp616
677 29 Paulson, J. N., Stine, O. C., Bravo, H. C. & Pop, M. Differential abundance analysis for
678 microbial marker-gene surveys. *Nat Methods* **10**, 1200-1202 (2013).
679 https://doi.org/10.1038/nmeth.2658
680 30 Mandal, S. *et al.* Analysis of composition of microbiomes: a novel method for studying
681 microbial composition. *Microb Ecol Health Dis* **26**, 27663 (2015).
682 https://doi.org/10.3402/mehd.v26.27663
683 31 Langille, M. G. *et al.* Microbial shifts in the aging mouse gut. *Microbiome* **2**, 50 (2014).
684 https://doi.org/10.1186/s40168-014-0050-9
685 32 Ziegler, T., Tsiountsioura, M., Meixner-Goetz, L., Cvirn, G. & Lamprecht, M. Polyphenols'
686 Impact on Selected Biomarkers of Brain Aging in Healthy Middle-Aged and Elderly Subjects: A
687 Review of Clinical Trials. *Nutrients* **15** (2023). https://doi.org/10.3390/nu15173770
688 33 Luo, J., Si, H., Jia, Z. & Liu, D. Dietary Anti-Aging Polyphenols and Potential Mechanisms.
689 *Antioxidants (Basel)* **10** (2021). https://doi.org/10.3390/antiox10020283
690 34 Xu, Q. *et al.* The flavonoid procyanidin C1 has senotherapeutic activity and increases
691 lifespan in mice. *Nat Metab* **3**, 1706-1726 (2021). https://doi.org/10.1038/s42255-021-
692 00491-8
693 35 Davinelli, S. & Scapagnini, G. Interactions between dietary polyphenols and aging gut
694 microbiota: A review. *Biofactors* **48**, 274-284 (2022). https://doi.org/10.1002/biof.1785

695 36 Rodriguez-Lopez, P. *et al.* Grape and Grape-Based Product Polyphenols: A Systematic
696 Review of Health Properties, Bioavailability, and Gut Microbiota Interactions. *Horticulturae* **8**,
697 583 (2022).
698 37 Franceschi, C., Garagnani, P., Parini, P., Giuliani, C. & Santoro, A. Inflammaging: a new
699 immune-metabolic viewpoint for age-related diseases. *Nat Rev Endocrinol* **14**, 576-590
700 (2018). https://doi.org/10.1038/s41574-018-0059-4
701 38 Cani, P. D., Depommier, C., Derrien, M., Everard, A. & de Vos, W. M. Author Correction:
702 Akkermansia muciniphila: paradigm for next-generation beneficial microorganisms. *Nat Rev*
703 *Gastroenterol Hepatol* **19**, 682 (2022). https://doi.org/10.1038/s41575-022-00650-6
704 39 Biagi, E. *et al.* Gut Microbiota and Extreme Longevity. *Curr Biol* **26**, 1480-1485 (2016).
705 https://doi.org/10.1016/j.cub.2016.04.016
706 40 Kong, F. *et al.* Gut microbiota signatures of longevity. *Curr Biol* **26**, R832-R833 (2016).
707 https://doi.org/10.1016/j.cub.2016.08.015
708 41 Biagi, E. *et al.* Through ageing, and beyond: gut microbiota and inflammatory status in
709 seniors and centenarians. *PLoS ONE* **5**, e10667 (2010).
710 https://doi.org/10.1371/journal.pone.0010667
711 42 Karygianni, L., Ren, Z., Koo, H. & Thurnheer, T. Biofilm Matrixome: Extracellular
712 Components in Structured Microbial Communities. *Trends Microbiol* **28**, 668-681 (2020).
713 https://doi.org/10.1016/j.tim.2020.03.016
714 43 Flemming, H. C. & Wingender, J. The biofilm matrix. *Nat Rev Microbiol* **8**, 623-633 (2010).
715 https://doi.org/10.1038/nrmicro2415
716 44 Maffei, V. J. *et al.* Biological Aging and the Human Gut Microbiota. *J Gerontol A Biol Sci Med*
717 *Sci* **72**, 1474-1482 (2017). https://doi.org/10.1093/gerona/glx042
718 45 Parker, A. *et al.* Fecal microbiota transfer between young and aged mice reverses hallmarks
719 of the aging gut, eye, and brain. *Microbiome* **10**, 68 (2022). https://doi.org/10.1186/s40168-
720 022-01243-w
721 46 Winter, S. E. *et al.* Host-derived nitrate boosts growth of E. coli in the inflamed gut. *Science*
722 **339**, 708-711 (2013). https://doi.org/10.1126/science.1232467
723 47 Sovran, B. *et al.* Age-associated Impairment of the Mucus Barrier Function is Associated
724 with Profound Changes in Microbiota and Immunity. *Sci Rep* **9**, 1437 (2019).
725 https://doi.org/10.1038/s41598-018-35228-3

726 48 Man, A. L. *et al.* Age-associated modifications of intestinal permeability and innate
727 immunity in human small intestine. *Clin Sci (Lond)* **129**, 515-527 (2015).
728 https://doi.org/10.1042/CS20150046
729 49 Wilms, E. *et al.* Intestinal barrier function is maintained with aging - a comprehensive study
730 in healthy subjects and irritable bowel syndrome patients. *Sci Rep* **10**, 475 (2020).
731 https://doi.org/10.1038/s41598-019-57106-2
732 50 Mezhibovsky, E. *et al.* Grape Polyphenols May Prevent High-Fat Diet-Induced Dampening
733 of the Hypothalamic-Pituitary-Adrenal Axis in Male Mice. *J Endocr Soc* **7**, bvad095 (2023).
734 https://doi.org/10.1210/jendso/bvad095
735 51 Roopchand, D. E. *et al.* Dietary Polyphenols Promote Growth of the Gut Bacterium
736 Akkermansia muciniphila and Attenuate High-Fat Diet-Induced Metabolic Syndrome.
737 *Diabetes* **64**, 2847-2858 (2015). https://doi.org/10.2337/db14-1916
738 52 Chacar, S. *et al.* The Impact of Long-Term Intake of Phenolic Compounds-Rich Grape
739 Pomace on Rat Gut Microbiota. *J Food Sci* **83**, 246-251 (2018). https://doi.org/10.1111/1750-
740 3841.14006
741 53 Ramos-Romero, S. *et al.* Modifications of Gut Microbiota after Grape Pomace
742 Supplementation in Subjects at Cardiometabolic Risk: A Randomized Cross-Over Controlled
743 Clinical Trial. *Foods* **9** (2020). https://doi.org/10.3390/foods9091279
744

745

746 **Figure 1.**

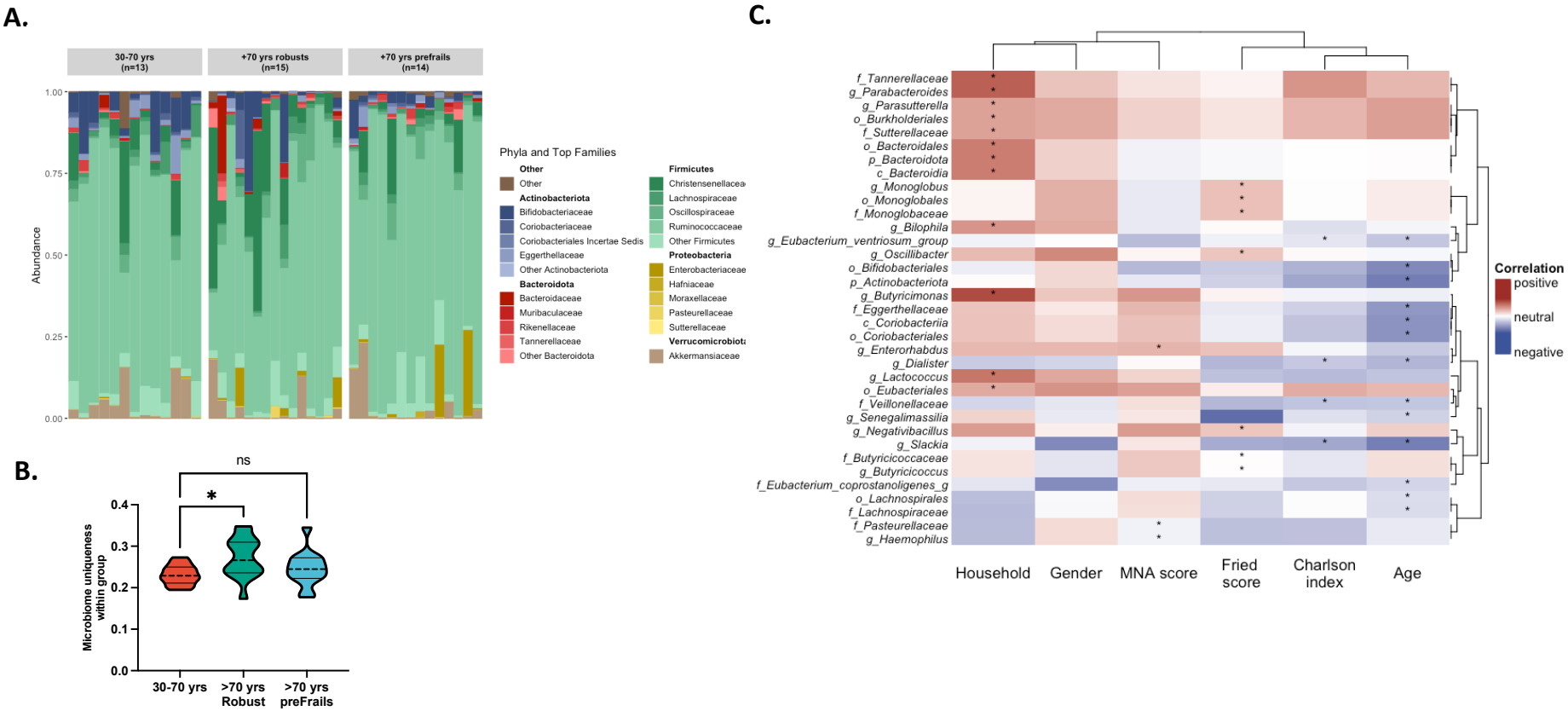

747

Figure 2.

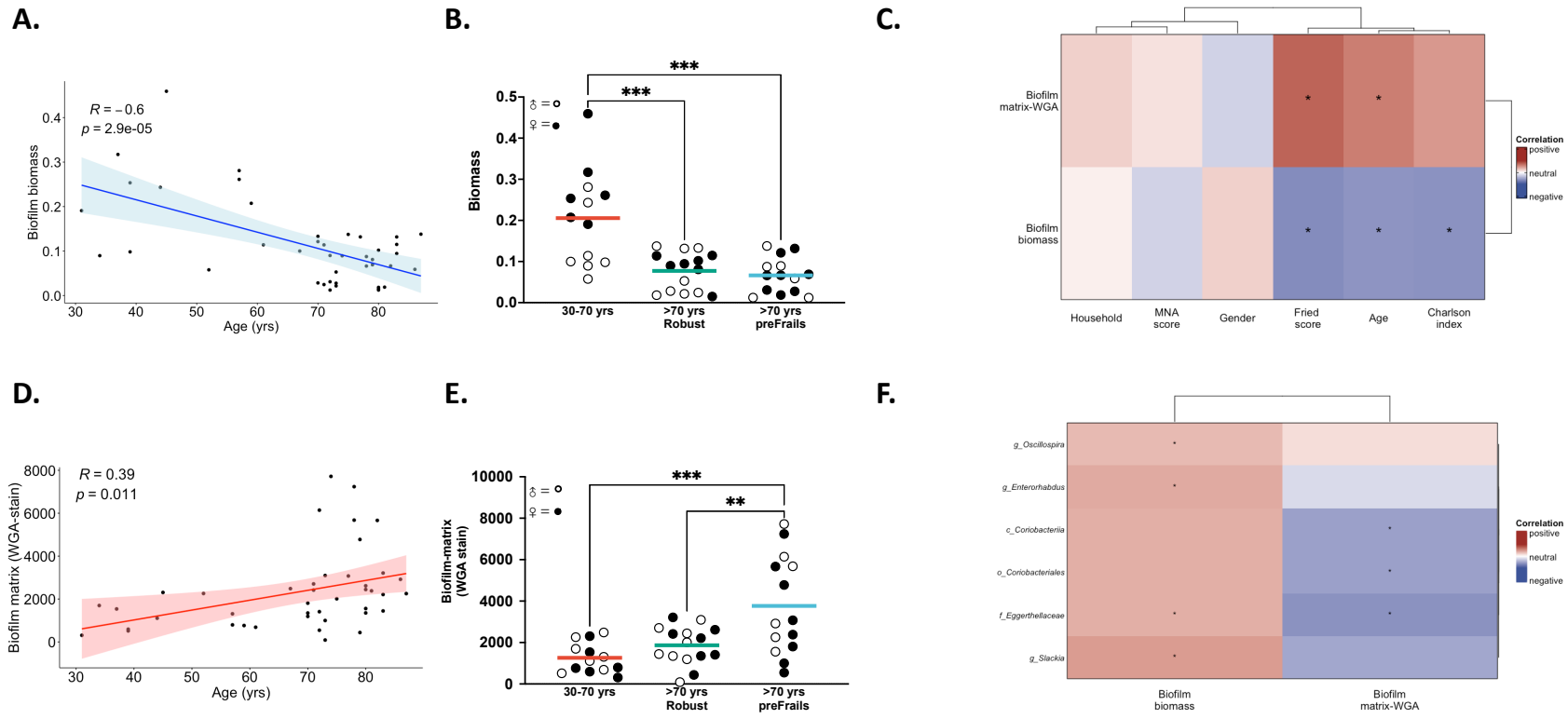
A.
R = −0.6
p = 2.9e-05
Biofilm biomass
Age (yrs)
B.
Biomass
30-70 yrs
>70 yrs Robust
>70 yrs preFrails
C.
Biofilm matrix-WGA
Biofilm biomass
Household
MNA score
Gender
Fried score
Age
Charlson index
Correlation
positive
neutral
negative
D.
R = 0.39
p = 0.011
Biofilm matrix (WGA-stain)
Age (yrs)
E.
Biofilm-matrix (WGA stain)
30-70 yrs
>70 yrs Robust
>70 yrs preFrails
F.
g_Oscillospira
g_Enterorhabdus
c_Coriobacteria
o_Coriobacteriales
f_Eggerthellaceae
g_Slackia
Biofilm biomass
Biofilm matrix-WGA
Correlation
positive
neutral
negative

751

752 **Figure 3.**

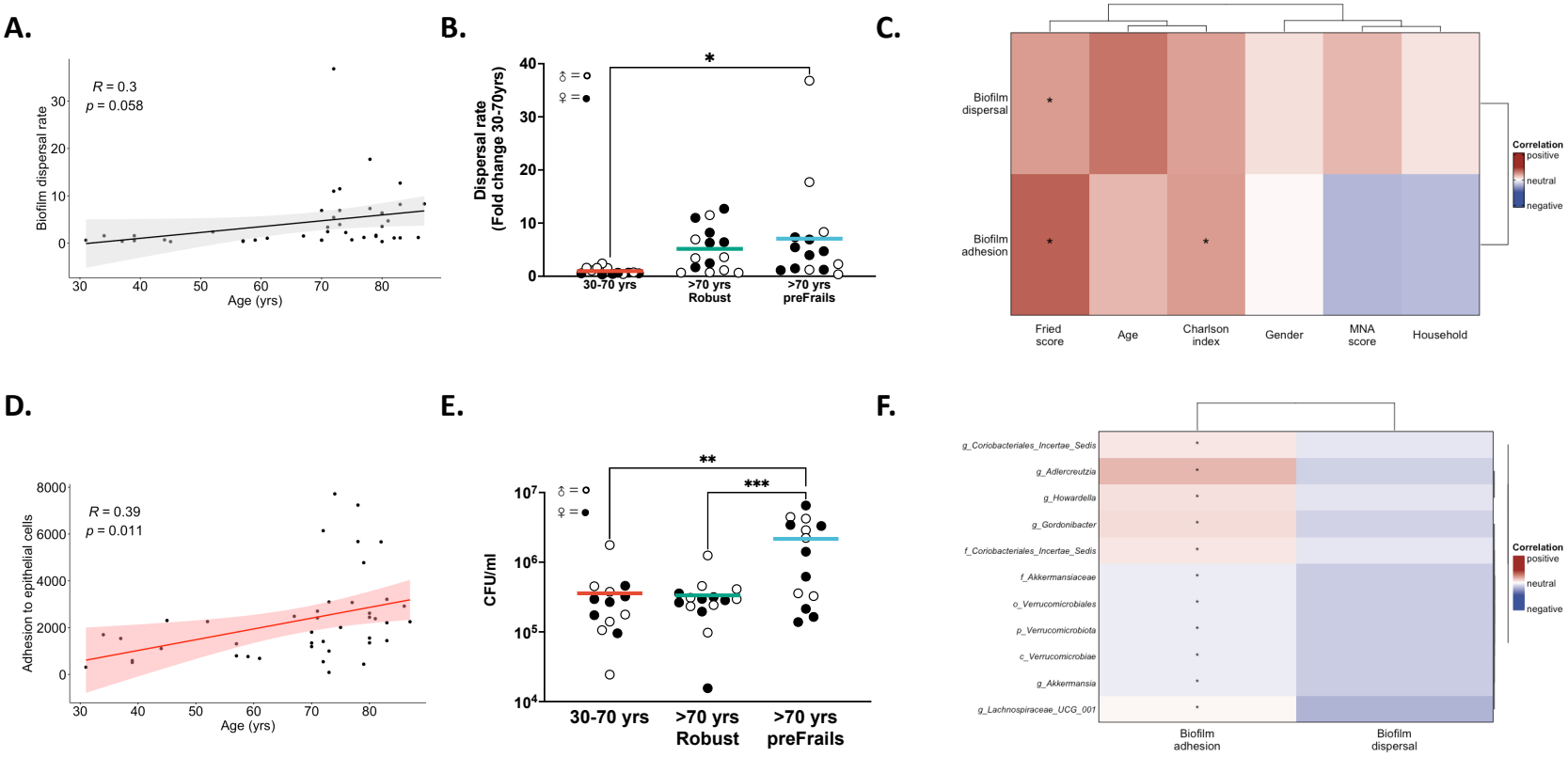

753

Figure 4.

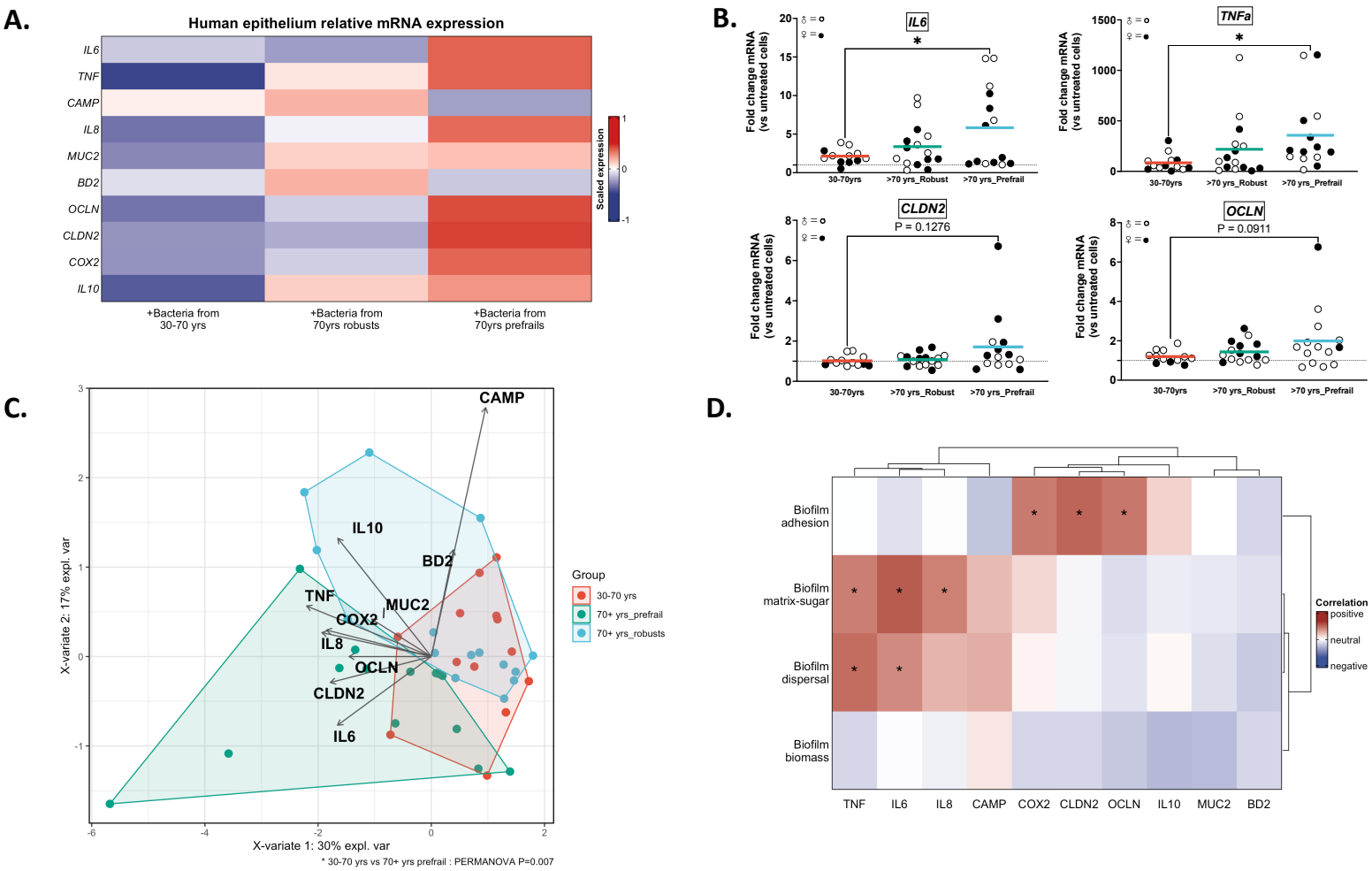
A.
Human epithelium relative mRNA expression
IL6
TNF
CAMP
IL8
MUC2
BD2
OCLN
CLDN2
COX2
IL10
+Bacteria from 30-70 yrs
+Bacteria from 70yrs robusts
+Bacteria from 70yrs prefrails
Scaled expression
B.
IL6
TNFa
CLDN2
P = 0.1276
OCLN
P = 0.0911
Fold change mRNA (vs untreated cells)
30-70yrs
>70 yrs_Robust
>70 yrs_Prefrail
C.
CAMP
IL10
BD2
TNF
MUC2
COX2
IL8
OCLN
CLDN2
IL6
X-variate 1: 30% expl. var
X-variate 2: 17% expl. var
Group
30-70 yrs
70+ yrs_prefrail
70+ yrs_robusts
* 30-70 yrs vs 70+ yrs prefrail : PERMANOVA P=0.007
D.
Biofilm adhesion
Biofilm matrix-sugar
Biofilm dispersal
Biofilm biomass
TNF
IL6
IL8
CAMP
COX2
CLDN2
OCLN
IL10
MUC2
BD2
Correlation
positive
neutral
negative

Figure 5.

Figure 6.

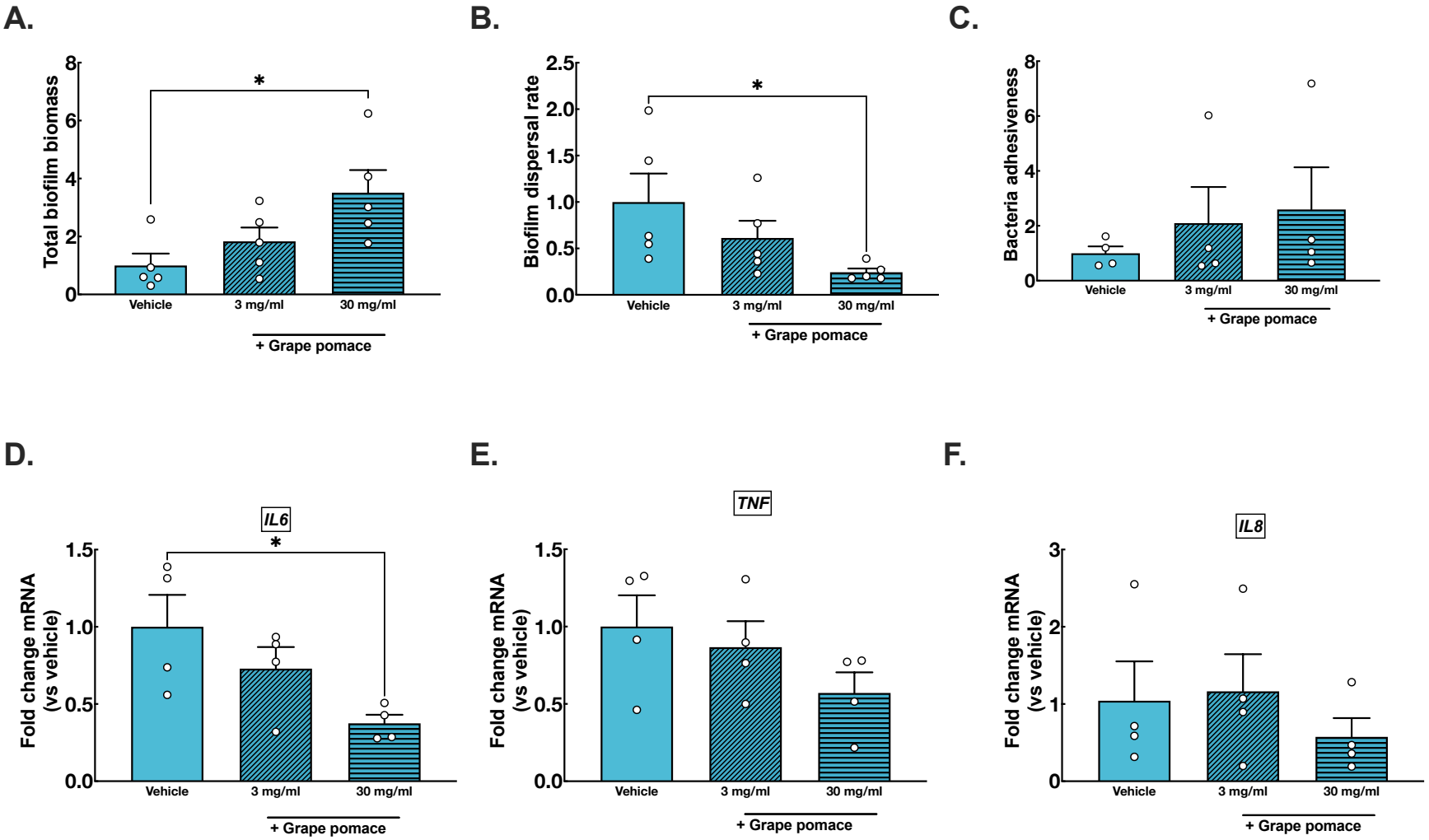
A.
Total biofilm biomass
8
6
4
2
0
*
Vehicle
3 mg/ml
30 mg/ml
+ Grape pomace
B.
Biofilm dispersal rate
2.5
2.0
1.5
1.0
0.5
0.0
*
Vehicle
3 mg/ml
30 mg/ml
+ Grape pomace
C.
Bacteria adhesiveness
8
6
4
2
0
Vehicle
3 mg/ml
30 mg/ml
+ Grape pomace
D.
IL6
Fold change mRNA (vs vehicle)
1.5
1.0
0.5
0.0
*
Vehicle
3 mg/ml
30 mg/ml
+ Grape pomace
E.
TNF
Fold change mRNA (vs vehicle)
1.5
1.0
0.5
0.0
Vehicle
3 mg/ml
30 mg/ml
+ Grape pomace
F.
IL8
Fold change mRNA (vs vehicle)
3
2
1
0
Vehicle
3 mg/ml
30 mg/ml
+ Grape pomace

763

764

765 **Table 1.**

	Adults (30-70 yrs) (n=13)	>70yrs robusts (n=15)	>70yrs prefrails (n=14)	p
Gender				0.846
Male	7 (53.8)	6 (42.9)	7 (46.7)	
Female	6 (46.2)	8 (57.1)	8 (53.3)	
Mean age (years)	47.8 (±11.6)	77.8 (±5.21)[1]	76.2 (±5.07)	**< 0.001**
Household status				0.786
Solo	9 (69.2)	10 (71.4)	9 (60)	
With partner	4 (30.8)	4 (28.6)	6 (40)	
Mean Fried Frailty Index	0 (±0)	0 (±0)[2]	1.14 (±0.363)	**< 0.001**
Mean Charlson Comorbidity Index	0.923 (±1.19)	5.07 (±1.59)[3]	4.73 (±1.87)	**< 0.001**
Mean MNA score	27.7 (±1.58)	28.1 (±1.27)	27.5 (±2.30)	0.713

766

767 **Figure and Table legends.**

768 **Figure 1: Taxonomic analyses of biofilms from human aging cohort.** Fecal microbiota
769 cultured *in vitro* on a polymicrobial anaerobic biofilm model underwent 16S rRNA V3-V4 gene
770 sequencing. The study groups include individuals aged 30-70 years (n=13), individuals aged
771 70 years and above characterized as healthy aging (robust, n=15) and +70 years prefrail
772 (n=14). **A.** The stacked bar plots illustrate the relative abundance of the 5 major Phyla and
773 their top 5 most abundant Families. Each individual is depicted as a separate bar plot,
774 highlighting taxonomic variations **B.** For each individual, the average of lowest values from
775 four different beta-diversity matrices (Bray-Curtis, Jaccard, unifrac, and weighted unifrac)
776 represented individual uniqueness. Statistical significance was determined by ANOVA
777 followed by Tukey's for multiple comparisons, where P<0.05 was considered significant (*
778 for P< 0.05, *** for P<0.0010). **C.** Heatmap represents Kendall's correlation coefficients
779 between biofilm taxa counts clinical parameters from human donors. Clinical parameters
780 include discrete and continuous clinical features: household (1: solo 2: with a partner),
781 gender (1: male, 2: female), MNA score, Charlson index, age, and Fried Frailty Index. The
782 color gradient from blue to red signifies negative to positive correlations, and * corresponds
783 to Kendall's P value <0.05. For enhanced clarity, the heatmap was filtered to include only
784 significantly positive or negative correlations (P<0.05).

785 **Figure 2. Prefrailty associated microb-aging is linked with physical alterations of human**
786 **biofilms.** Feces from individuals aged 30-70 years, 70+ years robust, and 70+ years prefrail,
787 were cultured *in vitro* as a polymicrobial anaerobic biofilm. **(A-B)** The total biofilm biomass
788 and **(D-E)** and the total sialic acid/N-acetylglucosamine glycoproteins content of extracellular
789 biofilm matrix were measured with WGA stain. **(A-D)** Pearson correlation relationship
790 between biofilm measures (biomass in **A.**, WGA-matrix in **D.**) and donor's age are presented.

791 Shaded area around the regression line represents the 95% confidence interval. **(B-E)** Scatter
792 plots depict for each individual's its corresponding value of biofilm biomass (in **B.**) and biofilm
793 WGA-matrix (in **E.**) and were grouped for each three cohort of individuals. In panels B and E
794 each dot is the average value of an individual donor biofilm (at least 12 replicates). The
795 gender of each donor is indicated using open(male)/filled(female) circles. Statistical
796 significance was determined by ANOVA followed by Tukey's for multiple comparisons, where
797 P<0.05 was considered significant. **(C-F)** Heatmaps represent Kendall (in **F.**) or Pearson (in **C.**)
798 correlation coefficients between biofilm physical structure and clinical data (in **C.**) or biofilm
799 taxa counts (in **F.**). Clinical parameters include discrete and continuous clinical features:
800 household (1: solo 2: with a partner), gender (1: male, 2: female), MNA score, Charlson index,
801 age, and Fried Frailty Index. The color gradient ranges from blue (negative) to red (positive)
802 correlations, with statistically significant associations (P<0.05) marked with *. For enhanced
803 clarity, the heatmap in panel **F.** was filtered to include only taxa rank with significantly
804 positive or negative correlations (P<0.05).

805 **Figure 3. Prefrailty associated microb-aging is linked with pathogenic traits of human**
806 **biofilms.** Feces from individuals aged 30-70 years, 70+ years robust, and 70+ years prefrail,
807 were cultured *in vitro* as a polymicrobial anaerobic biofilm. **(A-B)** The rate of dispersal of
808 planktonic bacteria, biofilm-dispersed bacteria, during a 24-hour period from biofilms was
809 measured. Raw values were normalized to the average dispersal rate of the 30-70 years
810 group. **(D-E)** Normalized counts of biofilm-dispersed bacteria were cultured on the apical
811 surface of the human Caco2/HT29MTX monolayer. After a 4-hour coculture, the number of
812 bacteria adhered to the epithelium was quantified. **(A-D)** Pearson correlations between
813 biofilm rate of dispersal (in **A.**) or adhesiveness (in **D.**) with the age of donors is presented.
814 **(B-E)** Scatter plots depict for each individual's its corresponding value of biofilm dispersal

815 rate (in **B.**) or adhesiveness (in **E.**) and were grouped for each three cohort of individuals. In
816 panels B and E each dot is the average value of an individual donor biofilm (at least 12
817 replicates). The gender of each donor is indicated using open(male)/filled(female) circles.
818 Statistical significance was determined by ANOVA followed by Tukey's for multiple
819 comparisons, where P<0.05 was considered significant. **(C-F)** Heatmaps represent Kendall (in
820 **F.**) or Pearson (in **C.**) correlation coefficients between biofilm pathogenic traits and clinical
821 data (in **C.**) or biofilm taxa counts (in **F.**). Clinical parameters include discrete and continuous
822 clinical features: household (1: solo 2: with a partner), gender (1: male, 2: female), MNA
823 score, Charlson index, age, and Fried Frailty Index. The color gradient ranges from blue
824 (negative) to red (positive) correlations, with statistically significant associations (P<0.05)
825 marked with *. For enhanced clarity, the heatmap in panel **F.** was filtered to include only taxa
826 rank with significantly positive or negative correlations (P<0.05).

827 **Figure 4. Increased host epithelial inflammatory response to prefrailty-associated human**
828 **biofilms.** After coculture with a normalized amount of biofilm-dispersed bacteria, epithelial
829 cells were collected for RNA extraction. **A.** The heatmap represents scaled relative expression
830 of a targeted list of host response genes. Specifically, these genes are involved in innate
831 inflammatory signaling (*IL6*, *TNF*, *IL8*, *IL10*, *COX2*, and *BD2*), secretion (*BD2* and *MUC2*), and
832 tight junction function (*OCLN* and *CLDN2*). The color gradient from blue to red correspond to
833 scale relative mRNA expression. **B.** Scatter plot depicts relative mRNA expression of *IL6*, *TNF*,
834 *CLDN2* and *OCLN* for each individual's and were grouped for each three cohort of individuals.
835 The gender of each donor is indicated using open(male)/filled(female) circles. Dotted line at
836 1 corresponds to basal mRNA expression in wells without bacteria. Statistical significance
837 was determined by ANOVA followed by Tukey's for multiple comparisons, where P<0.05 was
838 considered significant. **C.** Gene expression dataset was ordinated using Partial least squares-

839 discriminant analysis (PLS-DA) with its corresponding loading vectors. Pairwise PERMANOVA
840 revealed statistical differences between the group of 30-70 years and +70 years prefrail
841 (P=0.007). **D.** The heatmap corresponds to Pearson correlation coefficients between host
842 epithelial gene response and biofilm features. The color gradient from blue to red signifies
843 negative to positive correlations, and * corresponds to Pearson P value <0.05.

844 **Figure 5. Prefrailty aging in mice is linked with altered gut biofilm and emergence of**
845 **pathogenic behavior when transferred into recipient mice. (A-C.)** Using 16S fluorescent *in*
846 *situ* hybridization, we visualized tissue-associated microbiota in the distal colon of young (6
847 months, 6M, n=8, **A.**), aged (24 months, 24M) robust (n=7, **B.**), and aged prefrail (n=7, **C.**)
848 mice. Representative images are presented with blue is DAPI staining for host nuclei, green
849 is fluorescein-coupled wheat germ agglutinin for glycoproteins-rich content (e.g., mucus
850 layer), and red is the 16S-Cyanine3 probe for all bacteria. Dashed lines represent the limits
851 of mucosal tissue and the "inner mucus layer". Arrows highlight areas of interest. Scale bars
852 are 25 µm. **D.** Biofilm-damage scores were calculated for the three groups of mice, with dots
853 representing the mean score from at least 3 fields per animal. **(E-G.)** C57Bl/6 animals (8
854 weeks old) were previously exposed to 10-day antibiotics and underwent oral gavage with
855 either vehicle (PBS, n=5), or with feces from young (6M, n=9), aged robust (24M robust, n=8),
856 and aged prefrail (24M prefrail, n=7) mice. **E.** Four days after inoculation, feces were
857 collected for microbial taxonomy assessment using 16S rRNA V3-V4 gene sequencing. Colons
858 were harvested for (**F.**) parietal thickness measurement and (**G.**) macroscopic damage score.
859 **(D, F, G)** Bar plots corresponds to mean value per group ±SEM. Statistical significance was
860 determined by ANOVA followed by Dunnett's for multiple comparisons, where P<0.05 was
861 considered significant (* for P<0.05, ** for P<0.01).

862 **Figure 6 Positive impact of grape pomace on prefrailty-associated human biofilm structure**
863 **and virulence.** Polymicrobial anaerobic biofilms were generated from human feces of
864 prefrails individuals aged >70yrs, n=4-5 per group) and exposed to grape pomace diluted in
865 microbial broth at concentrations of 3 to 30 mg/ml for 24 hours. **A.** Total biomass was
866 evaluated using safranin-O stain, and the data are presented as the fold change of mean
867 biomass from control prefrail biofilms (broth media). **B.** The rate of dispersal for each biofilm
868 was evaluated as a ratio between amount of biofilm-dispersed bacteria and biofilm biomass
869 previously assessed. **C.** Normalized counts of biofilm-dispersed bacteria were cultured on the
870 apical surface of the human Caco2/HT29MTX monolayer. After a 4-hour coculture, the
871 number of bacteria adhered to the epithelium was quantified by plating and was represented
872 as fold change of vehicle treated biofilms (broth media). **D-F**. Dispersed bacteria were
873 collected from biofilms previously exposed to grape pomace. Human intestinal epithelial cell
874 lines (Caco2 and HT29MTX, at a 3:1 ratio) were then exposed to these bacteria for 4 hours,
875 and mRNA expression of *IL6* (**D.**), *TNF* (**E.**) and *IL8* (**F.**) genes were assessed. **(A-C)** Bar plots
876 corresponds to average value ± SEM of 12 biofilm replicates from human donors
877 (represented as individual dots). **(D-F)** Bar plots corresponds to average value ± SEM of
878 relative mRNA expression of vehicle control group (n=4 human donors). Statistical
879 significance was determined by ANOVA followed by Dunnett's for multiple comparisons,
880 where P<0.05 was considered significant and * for P<0.05 and *** for P<0.001.
881 **Table 1. Human cohort characteristics.** Data are represented as mean (± standard deviation)
882 for continuous variables and n (%) for categorical variables. MNA: Mini nutritional
883 assessment. Statistical significance was determined by ANOVA (Fisher test) followed by
884 Tukey's for multiple comparisons for continuous variables and Chi squared test for
885 categorical variables, where P<0.05 was considered significant. [1] Prefrail vs robust (p= 0.846)

886 and Prefrail vs Adults ($p < 0.001$), [2] Prefrail vs robust ($p < 0.001$) and Prefrail vs Adults ($p <$

887 0.001), [3] Prefrail vs robust ($p = 0.836$) and Prefrail vs Adults ($p < 0.001$).